

Multi-Task Model Merging via Adaptive Weight Disentanglement

Feng Xiong^{1,2,3*}, Runxi Cheng^{1,4*}, Wang Chen^{1†}, Zhanqiu Zhang¹,
Yiwen Guo^{5†}, Chun Yuan⁴, Ruifeng Xu^{2,3†}

¹LightSpeed Studios, Tencent ²Peng Cheng Laboratory

³Guangdong Provincial Key Laboratory of Novel Security Intelligence Technologies

⁴Tsinghua Shenzhen International Graduate School ⁵Independent Researcher

{faris.xiong, rickywchen, zqzhang27, guoyiwen89, xurufeng.hitsz}@gmail.com
{crx23, yuanc}@sz.tsinghua.edu.cn

Abstract

Model merging has gained increasing attention as an efficient and effective technique for integrating task-specific weights from various tasks into a unified multi-task model without retraining or additional data. As a representative approach, Task Arithmetic (TA) has demonstrated that combining task vectors through arithmetic operations facilitates efficient capability transfer between different tasks. In this framework, task vectors are obtained by subtracting the parameter values of a pre-trained model from those of individually fine-tuned models initialized from it. Despite the notable effectiveness of TA, interference among task vectors can adversely affect the performance of the merged model. In this paper, we relax the constraints of Task Arithmetic Property and propose Task Consistency Property, which can be regarded as being free from task interference. Through theoretical derivation, we show that such a property can be approximately achieved by seeking orthogonal task vectors. Guiding by this insight, we propose Adaptive Weight Disentanglement (AWD), which decomposes traditional task vectors into a redundant vector and several disentangled task vectors. The primary optimization objective of AWD is to achieve orthogonality among the disentangled task vectors, thereby closely approximating the desired solution. Notably, these disentangled task vectors can be seamlessly integrated into existing merging methodologies. Experimental results demonstrate that our AWD consistently and significantly improves upon previous merging approaches, achieving state-of-the-art results. Our code is available at <https://github.com/FarisXiong/AWD.git>.

1. Introduction

As the pretraining-finetuning paradigm gains increasing popularity [38], the research community has witnessed a proliferation of finetuned models [20], typically derived from foundational models such as T5 [23], and CLIP [22], among others. However, these models are often finetuned on task-specific training data, which limits their capacity for out-of-domain generalization [25, 29, 30]. In diverse real-world applications, the independent deployment of multiple fine-tuned models increases storage costs and computational demands. While traditional multi-task learning methods can mitigate these issues, they typically necessitate concurrent training across multiple task-specific datasets. Nonetheless, managing original datasets incurs significant expenses and potential privacy risks [16]. Moreover, when confronted with new tasks, traditional multi-task learning methods necessitate training from scratch. Consequently, exploiting existing models to construct efficient multi-task models has become a crucial challenge.

Fortunately, model merging [10] has garnered growing attention as an economical and efficient method for obtaining multi-task models. This approach aims to merge multiple task-specific models, requiring no original training data or only a small amount of unlabeled data, thereby enabling the merged model to perform efficiently across diverse tasks [40]. As a foundational technique in this field, Ilharco et al. [10] introduced the concept of Task Arithmetic. Specifically, Task Arithmetic combines task vectors through arithmetic operations, facilitating the efficient transfer of capabilities among different tasks and thus enabling the construction of multi-task models. Here, task vectors are derived by computing the difference between the weights of fine-tuned models and the pre-trained model. However, related studies have indicated that task interference has become the main challenge for this method [21, 39]. Previ-

* Equal Contribution.

† Corresponding authors.

ous studies have proposed various techniques to mitigate this issue [8, 33, 39, 44]. Ties-Merging [39] addresses this challenge by pruning redundant parameters, resolving sign conflicts, and averaging parameters aligned along dominant directions. DARE [44] reduces merging conflicts through random parameter drop and maintains model performance via rescaling operations. Consensus Merging [33] aims to eliminate selfish and catastrophic weights. Despite these advancements, these methods often rely on empirical strategies to resolve conflicts. In contrast, we clearly formulate the solution of model merging and derive a principled way for reducing interference between tasks.

In this paper, we revisit the Task Arithmetic Property and find that solving for task vectors satisfying this property in post-hoc methods is challenging. To more effectively guide task vector refinement, we propose the Task Consistency Property from the perspective of the merged model’s performance. Specifically, this property requires that the performance of the merged model on each task should be close to that achieved when only the corresponding task vector is incorporated. In this view, networks that satisfy this property can be considered as being free from interference between tasks. Through theoretical derivation, we show that task consistency property can be approximately achieved by seeking orthogonal task vectors. This solution is also partially supported by the experimental phenomenon of prior studies [10, 27], which indicate that a smaller cosine similarity between task vectors leads to reduced interference among them, thereby enhancing the performance of the merged model. Based on the previous discussions, we propose **Adaptive Weight Disentanglement (AWD)**. AWD aims to decompose traditional task vectors into a redundant vector and several disentangled task vectors, ensuring the disentangled task vectors can (1) exhibit enhanced orthogonality mutually while (2) maintaining the performance of specific tasks. It achieves these two characteristics by two key optimization objectives respectively: (1) minimizing the cosine similarity of the disentangled task vectors; and (2) minimizing the norm of the redundant vector. Furthermore, AWD can be seamlessly integrated into existing merging methods, such as Task Arithmetic [10] and AdaMerging [42].

Extensive experimental validations have demonstrated AWD’s effectiveness, and outperform existing merging techniques under various circumstances. When integrated with TA, AWD achieved absolute improvements in average accuracy of 2.8% on the ViT-B/32 model and 1.5% on the ViT-L/14 model compared to the advanced merging methods Ties-Merging. Moreover, we conducted further analyses, demonstrating that our method generalizes effectively on language models and exhibits enhanced robustness under various conditions. In summary, the main contributions of this research can be summarized as follows:

- We revisit Task Arithmetic Property and propose Task Consistency Property. Through theoretical derivation, we derive that task vectors are mutually orthogonal is a computationally tractable particular solution of this property.
- We propose Adaptive Weight Disentanglement to obtain disentangled task vectors, which could significantly enhance the performance of existing model merge methods.
- Extensive evaluations on vision models and language models across multiple benchmarks validate the effectiveness and generalizability of our method.

2. Related Work

Orthogonal Optimization in Continual Learning: The primary challenge in continual learning is enabling models to acquire the capability of new tasks without forgetting previously learned knowledge [34]. Recent studies [6, 7, 15, 35, 46] have demonstrated that maintaining the orthogonality of gradients during parameter updates can effectively mitigate interference with previous tasks in continual learning. Zeng et al. [46] introduced an optimization technique based on orthogonal projection, which effectively reduces forgetting by projecting the gradient of new tasks onto the orthogonal subspace of the gradient of previous tasks during parameter updates. Similarly, Farajtabar et al. [6] proposed Orthogonal Gradient Descent with Memory, enhancing the continual learning capability of models by integrating a memory replay mechanism. Saha and Roy [24] introduce a scaled gradient projection method that integrates orthogonal projection with scaled updates along significant past gradients, thereby achieving enhanced task generalization with minimal forgetting. Wang et al. [35] propose optimizing LoRA within the orthogonal subspace to preserve the generalization capabilities. Orthogonal optimization methods have demonstrated unique advantages for avoiding parameter and gradient conflict in continual learning. From this perspective, orthogonal task vectors can be further considered as a potential solution to model merging, as exemplified by our AWD approach.

Multi-task Model Merging: Model merging encompasses a diverse set of methodologies, including weight alignment [1, 12], architectural transformation [31], multi-task learning [10, 21], knowledge editing [2], and other related techniques [40]. In this paper, we concentrate on the multi-task model merging, which can be categorized into pre-hoc and post-hoc approaches. **For pre-hoc methods:** Pre-hoc methods advocate modifying the model’s training procedure prior to training to enhance weight disentanglement. Ortiz-Jimenez et al. [21] established a connection between Task Arithmetic [10] and the spatial localization of NTK eigenfunctions, providing a method through NTK linearization to amplify weight disentanglement. Building on this insight, Tang et al. [28] proposed L-LoRA, that partially linearizes adapter modules and applies arithmetic opera-

tions to the linearized adapters. This approach leverages the advantages of linearized fine-tuning for model merging while efficiently performing both fine-tuning and inference. **For post-hoc methods:** Early merging methods primarily focused on integrating individual models. Simple Averaging [36] constructs the merged weights by independently computing the arithmetic mean of each corresponding parameter across all models. Fisher Merging [19] performs weighted parameter fusion by utilizing the fisher information matrix to assess the importance of individually fine-tuned model parameters. RegMean [11] addresses model merging by minimizing the predictive discrepancies between the merged model and the task-specific models. Recently, Ilharco et al. [10] demonstrated that efficient capability transfer can be achieved by combining task vectors through arithmetic operations. However, task interference remains a significant challenge. Ties-Merging [39] resolves this challenge by trimming redundant parameters, resolving the sign conflicts, and averaging parameters that align with the predominant direction. DARE [44] mitigates merging conflicts by randomly dropping parameters and preserves model performance through essential unscaling operations. Consensus Merging [33] eliminates selfish and catastrophic weights, thereby enhancing the overall performance of existing model merging methods while simultaneously compressing the model. In our work, we have demonstrated that the orthogonality among task vectors is the key to improving performance in model merging and introducing adaptive weight disentanglement to improve orthogonality.

3. Methodology

3.1. Preliminary of Multi-task Model Merging

Notations: Formally, we define the weights of pre-trained model by Θ , which is initially trained on large-scale datasets to acquire general capabilities. Consider K tasks, for each task, the pre-trained parameters Θ are fine-tuned using a domain-specific training dataset, resulting in task-specific model sets denoted as $\mathcal{M} = \{\Theta_i^*\}_{i=1}^K$.

Task Vectors: Building on this, Ilharco et al. [10] define the task vector $\tau_i = \Theta_i^* - \Theta$, which represents the task-specific adaptations from the fine-tuning process. We define the task vectors set as $\mathcal{T} = \{\tau_i\}_{i=1}^K$.

Multi-task Model Merging: The objective of multi-task model merging is to combine the task-specific models set $\{\Theta_i^*\}_{i=1}^K$ into a unified model $\hat{\Theta}$, or to merge the task vectors \mathcal{T} into the pre-trained model Θ . The merged model $\hat{\Theta}$ aims to generalize effectively across all K tasks, without resorting to approaches such as retraining from scratch or requiring full access to the training datasets of all tasks. Following Ilharco et al. [10], Matena and Raffel [19], Yadav et al. [39], we focus on merging task vectors into the pre-trained model.

Task Arithmetic Property: In context of multi-task model merging, we aspire adding task vector will not affect the output in other domains, which is defined as Task Arithmetic Property by Ortiz-Jimenez et al. [21].

Property 1 (Task Arithmetic Property). *Given coefficient sets $\{\lambda_i\}_{i=1}^K \subset \mathbb{R}$ and a set of task vectors $\mathcal{T} = \{\tau_i\}_{i=1}^K$ correspond with non-intersecting task-specific data supports $\mathcal{D} = \{\mathcal{D}_i\}_{i \in [K]}$, i.e., $\forall t, t', \text{ if } t \neq t' \text{ then } \mathcal{D}_t \cap \mathcal{D}_{t'} = \emptyset$. We say a network f satisfies the task arithmetic property around Θ with respect to \mathcal{T} and \mathcal{D} if:*

$$f\left(x; \Theta + \sum_i^K \lambda_i \tau_i\right) = \begin{cases} f(x; \Theta + \lambda_i \tau_i) & x \in \mathcal{D}_i \\ f(x; \Theta) & x \notin \bigcup_{i=1}^K \mathcal{D}_i \end{cases} \quad (1)$$

3.2. Theoretical Analysis

In an ideal scenario, we desire the network to possess task arithmetic property 1. Given that the output of a model typically depends on its input, it is challenging to retrospectively adjust the pre-trained model or task vectors to satisfy this property. Considering the fundamental requirement for model merging is that the merged model should demonstrate performance on each task comparable to that of its respective task-specific model, we propose the **Task Consistency Property**. Specifically, this property necessitates that the performance of the merged model on each task should be close to the performance achieved when only the corresponding task vector is integrated. In this context, the networks that satisfy task consistency property can be considered free from interference between tasks. Task consistency property can be regarded as a more relaxed extension of the task arithmetic property, but it aligns better with the goal of multi-task model merging and is easier to solve. Its formal expression is as follows:

Property 2 (Task Consistency Property). *Given coefficient sets $\{\lambda_i\}_{i=1}^K \subset \mathbb{R}$ and a set of task vectors $\mathcal{T} = \{\tau_i\}_{i=1}^K$ correspond with non-intersecting task-specific data supports $\mathcal{D} = \{\mathcal{D}_i\}_{i \in [K]}$, i.e., $\forall t, t', \text{ if } t \neq t' \text{ then } \mathcal{D}_t \cap \mathcal{D}_{t'} = \emptyset$. We say a network f satisfies the task consistency property around Θ with respect to \mathcal{T} and \mathcal{D} if:*

$$\forall \mathcal{D}_i \in \mathcal{D}, \mathcal{L}_i\left(\Theta + \sum_j^K \lambda_j \tau_j\right) = \mathcal{L}_i(\Theta + \lambda_i \tau_i), \quad (2)$$

where $\mathcal{L}_i(\cdot)$ denotes the loss function of task i . Property 1 and 2 are characteristics jointly manifested by the pre-trained model and the task vectors. Considering that the pre-trained model serves as the cornerstone of model merging [21], simultaneously editing both the pre-trained model and the task vectors would hinder the network’s ability to scale to new tasks. Therefore, we fix the pre-trained model and solve for the task vector that satisfies Property 2, which guides us in refining the task vector.

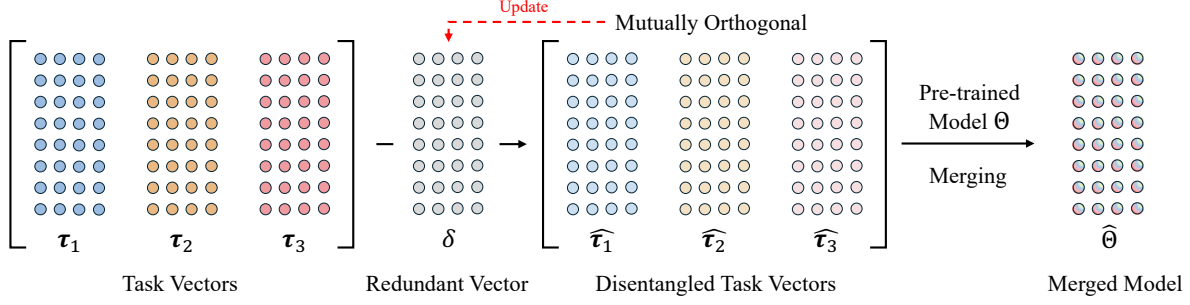


Figure 1. Illustration of our Adaptive Disentangled Weight.

To simplify Eq. 2, we formally define the Merging Gap G_i for task i as:

$$G_i = \mathcal{L}_i \left(\Theta + \sum_j^K \lambda_j \tau_j \right) - \mathcal{L}_i (\Theta + \lambda_i \tau_i). \quad (3)$$

Based on this, the task consistency property can be rewritten as follows,

$$\forall i, G_i = 0. \quad (4)$$

We then apply Taylor expansion around Θ on the right-hand side of Eq. 3. Given that the task vectors typically have small absolute values [44], terms of second-order and higher are generally negligible. Therefore, we use a first-order approximation and simplify the expression, which could be described as follows,

$$G_i \approx \left(\mathcal{L}_i (\Theta) + \left\langle \nabla_{\Theta} \mathcal{L}_i (\Theta), \sum_j^n \lambda_j \tau_j \right\rangle \right) \quad (5)$$

$$- (\mathcal{L}_i (\Theta) + \langle \nabla_{\Theta} \mathcal{L}_i (\Theta), \lambda_i \tau_i \rangle) \quad (6)$$

$$= \sum_{j \neq i}^K \langle \nabla_{\Theta} \mathcal{L}_i (\Theta), \lambda_j \tau_j \rangle. \quad (7)$$

Since the original data is often difficult to obtain or may not be accessible, calculating the gradient of the pre-trained model for a single task is challenging. As an alternative, we can replace this gradient with the task vector, as the task vector can be interpreted as the accumulation of gradients. Therefore, the gradient $\nabla_{\Theta} \mathcal{L}_i (\Theta)$ can be estimated as $k_i \tau_i$, where $k_i < 0$. Therefore, the merging gap G_i can be estimated as:

$$G_i \approx \sum_{j \neq i}^K \langle k_i \tau_i, \lambda_j \tau_j \rangle, \quad (8)$$

$$= k_i \sum_{j \neq i}^K \lambda_j \langle \tau_i, \tau_j \rangle. \quad (9)$$

Due to the inability to compute the magnitudes of the gradients, solving the aforementioned equation becomes challenging. As a result, we aim to find a particular solution for the equation. As shown in Eq. 9, when all task vectors are orthogonal to each other, Eq. 4 will be satisfied:

$$\forall i \neq j, \cos(\tau_i, \tau_j) = 0 \Rightarrow \forall i, G_i = 0. \quad (10)$$

Our derivation results are partially supported by the experimental phenomenon of previous studies [10, 27], which indicates that smaller positive cosine similarity leads to better performance in multi-task merging. Consequently, based on the aforementioned discussions, our work endeavors to identify a novel task vector set of $\hat{\mathcal{T}} = \{\hat{\tau}_1, \hat{\tau}_2, \dots, \hat{\tau}_K\}$, such that $\Theta + \hat{\tau}_i$ optimally restores the performance of the fine-tuned model Θ_i^* , while simultaneously enhancing the orthogonality between task vectors $\hat{\tau}_i$ and $\hat{\tau}_j$.

3.3. Adaptive Weight Disentanglement

Previous studies have shown that task vectors exhibit significant redundancy [39, 44]. By eliminating redundant components, some conflicts along the parameter directions can be avoided, which helps reduce interference between tasks. Inspired by this, our proposed AWD approach aims to identify and remove redundant vector from a set of task vectors to obtain more effective task vectors. As illustrated in Figure 1, when decomposing task vectors into redundant vector and disentangled task vectors, we expect the following characteristics could be satisfied. (1) **Orthogonality**: the disentangled task vectors exhibit smaller cosine similarity; (2) **Invariance**: the performance of the disentangled task vectors on their respective tasks remains comparable to that of the original task vectors. In this section, we define these two characteristics as our optimization objectives and utilize automatic differentiation tools to solve the aforementioned objectives **Adaptively**.

Formally, we define the redundant vector as δ , which is a trainable vector variable initialized to zero. By subtracting δ from each task vector, we obtain the disentangled task vectors set $\hat{\mathcal{T}} = \{\hat{\tau}_i\}_{i=1}^K$, where $\hat{\tau}_i = \tau_i - \delta$. Based on

this, the first optimization objective for **Orthogonality** can be expressed as:

$$\mathcal{L}_O = \frac{1}{K(K-1)} \sum_i^K \sum_{j \neq i}^K |\mathcal{F}(\hat{\tau}_i, \hat{\tau}_j)| \quad (11)$$

$$= \frac{1}{K(K-1)} \sum_i^K \sum_{j \neq i}^K |\mathcal{F}(\tau_i - \delta, \tau_j - \delta)|, \quad (12)$$

where \mathcal{F} denotes the cosines similarity function.

Besides, without proper constraints on δ , the disentangled task vector $\tau_i - \delta$ may experience a significant drop in performance on their corresponding tasks. This is because an excessively large redundant vector may remove information within the task vectors that is crucial for task performance. Recent studies have demonstrated that pruning the smaller components of the task vector has a negligible impact on model performance [39, 44]. Motivated by this insight, we introduce a norm constraint on δ and incorporate it as the second optimization objective for **Invariance**, which is formally expressed as:¹

$$\mathcal{L}_R = \|\delta\|. \quad (13)$$

Considering the above, our final optimization objective function can be expressed as a weighted sum of these two parts, formally,

$$\mathcal{L} = \mathcal{L}_O + \alpha \mathcal{L}_R, \quad (14)$$

where α is a hyperparameter used to balance the relationship between orthogonality and invariance. By minimizing the total loss, we can obtain the redundant vector $\delta = \arg \min_{\delta} \mathcal{L}(\delta; \mathcal{T})$. Then we can get the disentangled task vector by subtracting the redundant vector from the task vector $\hat{\tau}_i = \tau_i - \delta$.

Our approach can be seamlessly integrated into existing model merging approaches, including Task Arithmetic [10] and AdaMerging [42]. For **Task Arithmetic**: the final merged model $\hat{\Theta}$ can be formulated as $\hat{\Theta} = \Theta + \lambda \sum_i^K \hat{\tau}_i$. For **AdaMerging**: the final merged model $\hat{\Theta}$ can be formulated as $\hat{\Theta} = \Theta + \sum_i^K \sum_j^{\mathcal{P}} \lambda_{ij} \hat{\tau}_i^j$, where \mathcal{P} denotes the number of layers in $\hat{\tau}_i$, and $\hat{\tau}_i^j$ represents the parameter in j -th layer of $\hat{\tau}_i$.

4. Experiments

In this section, we will detail the experimental setup and the analysis of the results of this study. More detailed experimental data and additional analyses will be included in the Supplementary Materials.

¹Detailed proofs are provided in the supplementary materials.

Algorithm 1: Adaptive Weight Disentanglement

Input: Task Vectors $\mathcal{T} = \{\tau_i\}_{i=1}^K$; Solution Steps \mathcal{N} ; Learning Rate β ; Hyperparameter α .
Output: Disentangled Task Vectors $\hat{\mathcal{T}}$.

- 1 ▷ Initialize Redundant Vector δ^0 .
- 2 $\delta^0 \leftarrow 0$
- 3 **for** $n \in \{1, \dots, \mathcal{N}\}$ **do**
- 4 ▷ Initialize Total Loss \mathcal{L} .
- 5 $\mathcal{L} \leftarrow 0$
- 6 **for** $i \in \{1, \dots, K\}$ **do**
- 7 **for** $j \in \{1, \dots, K\}$ **do**
- 8 ▷ Calculate Loss by Redundant Vector and Task Vectors.
- 9 $\mathcal{L} += \mathcal{L}_O(\delta^{n-1}; \tau_i, \tau_j)$
- 10 $\mathcal{L} += \alpha \mathcal{L}_R$
- 11 ▷ Update the Redundant Vector δ^n .
- 12 $\delta^n = \delta^{n-1} - \beta \nabla_{\delta^{n-1}} \mathcal{L}(\delta^{n-1}; \mathcal{T})$
- 13 ▷ Calculate the Disentangled Task Vector.
- 14 $\hat{\mathcal{T}} = \{\tau_i - \delta^{\mathcal{N}}\}_{i=1}^K$

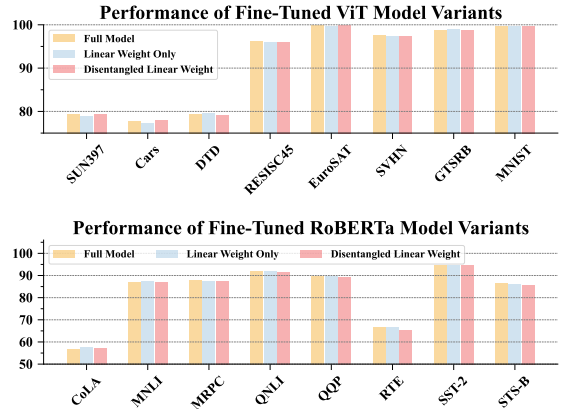


Figure 2. Comparative Performance of Fine-Tuned ViT-B/32 and RoBERTa Model Variants.

4.1. Experimental Settings

Datasets: Following the previous studies [10, 39, 41, 42], we explore multi-task model merging across eight image classification datasets: SUN397 [37], Cars [13], RE-SISC45 [3], EuroSAT [9], SVHN [45], GTSRB [26], MNIST [14], DTD [4].

Models: For our experiments, we employ the ViT-B/32 and ViT-L/14 models, originally derived from CLIP [22].

Baselines: To ensure a comprehensive evaluation, we categorize the baselines into three main groups: Non-merging methods, Training-free methods, and Test-time Adaptation methods. The Non-merging category includes individual finetuned models and traditional multi-task learning approaches. The training-free methods we consider

Table 1. Multi-task performance when merging ViT-B/32 models on 8-task vision benchmark. The best performance across different merging methods is denoted in bold.

| Method | SUN397 | Cars | RESISC45 | EuroSAT | SVHN | GTSRB | MNIST | DTD | Avg Acc |
|-----------------------------------|-------------|-------------|-------------|-------------|-------------|-------------|-------------|-------------|-------------|
| <i>Non-merging Methods</i> | | | | | | | | | |
| Pretrained | 62.3 | 59.7 | 60.7 | 45.5 | 31.4 | 32.6 | 48.5 | 43.8 | 48.0 |
| Individual | 79.2 | 77.7 | 96.1 | 99.7 | 97.5 | 98.7 | 99.7 | 79.4 | 90.8 |
| Traditional MTL | 73.9 | 74.4 | 93.9 | 98.2 | 95.8 | 98.9 | 99.5 | 77.9 | 88.9 |
| <i>Training-free Methods</i> | | | | | | | | | |
| Weight Averaging | 65.3 | 63.4 | 71.4 | 71.7 | 64.2 | 52.8 | 87.5 | 50.1 | 65.8 |
| Fisher Merging | 68.6 | 69.2 | 70.7 | 66.4 | 72.9 | 51.1 | 87.9 | 59.9 | 68.3 |
| RegMean | 65.3 | 63.5 | 75.6 | 78.6 | 78.1 | 67.4 | 93.7 | 52.0 | 71.8 |
| Task Arithmetic | 55.2 | 54.9 | 66.7 | 78.9 | 80.2 | 69.7 | 97.3 | 50.4 | 69.1 |
| Ties-Merging | 59.8 | 58.6 | 70.7 | 79.7 | 86.2 | 72.1 | 98.3 | 54.2 | 72.4 |
| Consensus Merging | 65.7 | 63.6 | 76.5 | 77.2 | 81.7 | 70.3 | 97.0 | 57.1 | 73.6 |
| AWD Task Arithmetic (Ours) | 63.5 | 61.9 | 72.6 | 84.9 | 85.1 | 79.1 | 98.1 | 56.7 | 75.2 |
| <i>Test-time Adaption Methods</i> | | | | | | | | | |
| TW AdaMerging | 58.0 | 53.2 | 68.8 | 85.7 | 81.1 | 84.4 | 92.4 | 44.8 | 71.1 |
| TW AdaMerging++ | 60.8 | 56.9 | 73.1 | 83.4 | 87.3 | 82.4 | 95.7 | 50.1 | 73.7 |
| LW AdaMerging | 64.5 | 68.1 | 79.2 | 93.8 | 87.0 | 91.9 | 97.5 | 59.1 | 80.1 |
| LW AdaMerging++ | 66.6 | 68.3 | 82.2 | 94.2 | 89.6 | 89.0 | 98.3 | 60.6 | 81.1 |
| Representation Surgery | 63.8 | 59.9 | 83.3 | 97.9 | 87.0 | 87.0 | 98.6 | 69.4 | 80.9 |
| AWD AdaMerging (Ours) | 68.1 | 71.4 | 83.4 | 94.8 | 87.7 | 93.6 | 97.9 | 66.1 | 82.9 |

Table 2. Multi-task performance when merging ViT-L/14 models on 8-task vision benchmark. The best performance across different merging methods is denoted in bold.

| Method | SUN397 | Cars | RESISC45 | EuroSAT | SVHN | GTSRB | MNIST | DTD | Avg Acc |
|-----------------------------------|-------------|-------------|-------------|-------------|-------------|-------------|-------------|-------------|-------------|
| <i>Non-merging Methods</i> | | | | | | | | | |
| Pretrained | 66.8 | 77.7 | 71.0 | 59.9 | 58.4 | 50.5 | 76.3 | 55.3 | 64.5 |
| Individual | 82.3 | 92.4 | 97.4 | 100 | 98.1 | 99.2 | 99.7 | 84.1 | 94.2 |
| Traditional MTL | 80.8 | 90.6 | 96.3 | 96.3 | 97.6 | 99.1 | 99.6 | 84.4 | 93.5 |
| <i>Training-free Methods</i> | | | | | | | | | |
| Weight Averaging | 72.1 | 81.6 | 82.6 | 91.9 | 78.2 | 70.7 | 97.1 | 62.8 | 79.6 |
| Fisher Merging | 69.2 | 88.6 | 87.5 | 93.5 | 80.6 | 74.8 | 93.3 | 70.0 | 82.2 |
| RegMean | 73.3 | 81.8 | 86.1 | 97.0 | 88.0 | 84.2 | 98.5 | 60.8 | 83.7 |
| Task Arithmetic | 73.9 | 82.1 | 86.6 | 94.1 | 87.9 | 86.7 | 98.9 | 65.6 | 84.5 |
| Ties-Merging | 76.5 | 85.0 | 89.3 | 95.7 | 90.3 | 83.3 | 99.0 | 68.8 | 86.0 |
| Consensus Merging | 75.0 | 84.3 | 89.4 | 95.6 | 88.3 | 82.4 | 98.9 | 68.0 | 85.2 |
| AWD Task Arithmetic (ours) | 76.2 | 85.4 | 88.7 | 96.1 | 92.4 | 92.3 | 99.3 | 69.4 | 87.5 |
| <i>Test-time Adaption Methods</i> | | | | | | | | | |
| AdaMerging | 79.0 | 90.3 | 90.8 | 96.2 | 93.4 | 98.0 | 99.0 | 79.9 | 90.8 |
| AdaMerging++ | 79.4 | 90.3 | 91.6 | 97.4 | 93.4 | 97.5 | 99.0 | 79.2 | 91.0 |
| Representation Surgery | 75.7 | 84.4 | 93.1 | 98.8 | 91.3 | 93.4 | 99.1 | 76.1 | 89.0 |
| AWD AdaMerging (Ours) | 79.8 | 90.6 | 91.8 | 97.0 | 93.9 | 98.4 | 99.2 | 81.1 | 91.5 |

are Weight Averaging [36], Fisher Merging [19], Reg-Mean [11], Task Arithmetic [10], Ties-Merging [39], and Consensus Merging [33]. Finally, we incorporate Test-time Adaptation methods, including AdaMerging [42] and Representation Surgery [41].

4.2. Pilot Experiment

Although our method is relatively simple, its applicability may still be limited when confronted with complex

transformer-based models, particularly when generalizing our approach to language models with high-dimensional embedding layers [43]. Dai et al. [5] suggest that knowledge neurons are stored within Feedforward Neural Networks. Inspired by this, we have further simplified our approach: restricting the parameters of the task vector solely to the weights of the linear layers within the transformer blocks. To validate the rationality of this simplified strategy, we conducted a series of pilot experiments. As shown

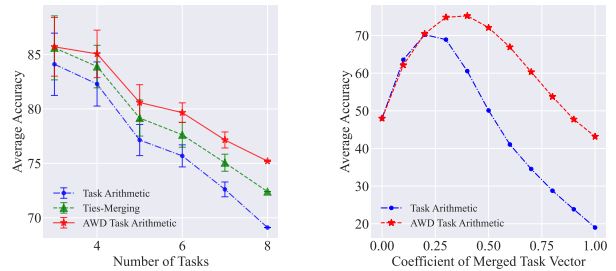
Table 3. Multi-task performance when merging RoBERTa models on 8-task GLUE benchmark. Following Lu et al. [18], we report average normalized score. Red text indicates the performance improvements compared to the most advanced baseline. The best performance across different merging methods is denoted in bold.

| Method | RoBERTa-Base | RoBERTa-Large |
|-----------------------------------|-----------------------------------|-----------------------------------|
| Pretrained | 41.7 | 38.2 |
| Individual | 100.0 | 100.0 |
| Weight Averaging | 52.6 | 53.3 |
| Task Arithmetic | 67.8 | 70.9 |
| Ties-Merging | 64.7 | 72.4 |
| Task Arithmetic (w/ DARE) | 63.7 | 70.9 |
| Ties-Merging (w/ DARE) | 65.6 | 72.8 |
| AWD Task Arithmetic (Ours) | 68.3Δ0.5 | 74.5Δ1.7 |

in Figure 2, whether in vision models or language models, we found that preserving only the parameters of weights in the linear layer of the task vector did not affect the performance of the models. Moreover, even after applying our method to combine with the disentangled task vector in this simplified variant, the models were able to recover to a performance level similar to that of the full fine-tuned models.

4.3. Main Results

The performance of all baselines using the ViT-B/32 and ViT-L/14 architectures is presented in Table 1 and Table 2, respectively. Our observations are as follows: (1) Our experiments demonstrate that individually fine-tuned models achieve the highest performance. Traditional multi-task learning approaches utilizing joint training exhibit slightly lower performance. (2) It is noteworthy that compared to previous merging methods, our strategy demonstrates significant performance improvements in consistency. By integrating Task Arithmetic, our approach achieves a notable improvement over the advanced method of Ties-Merging, outperforming it by 2.8% on the ViT-B/32 model and by 1.5% on the ViT-L/14 model. Moreover, in the test-time adaptation setting, by incorporating AdaMerging, our approach outperforms AdaMerging++ by 1.8% on ViT-B/32 and by 0.5% on ViT-L/14. (3) As model sizes increase, the performance of merging methods progressively aligns with that of traditional multi-task learning methods. Our approach demonstrates consistent improvements. Specifically, on ViT-L/14, under the test-time adaptation setting, it achieves performance that is only 2% lower than that of traditional multi-task learning. (4) Compared to test-time adaptation, our method demonstrates a more significant performance improvement in training-free scenarios. We attribute this phenomenon to the dynamic adjustment of task coefficients within the test adaptation setting. Specifically, the coefficients of task vectors can be interpreted as indicators of each task vector’s relative importance. Therefore, when the coefficients of task vectors change, it is appro-



(a) Average Accuracy Across Different Task Numbers (b) Average Accuracy Across Different Coefficients on 8 vision tasks

Figure 3. Impact of task numbers and coefficients on average accuracy for ViT-B/32.

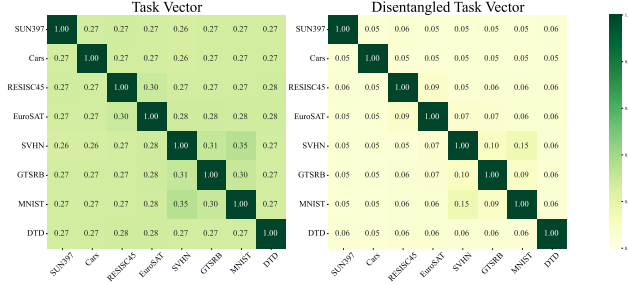
priate to adjust the weight distribution in the optimization objective accordingly.

4.4. Generalizability on Language Models

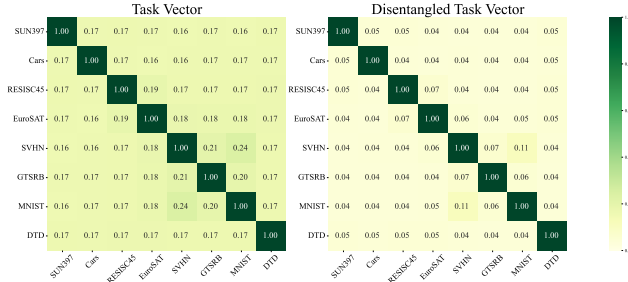
We further extend our methodology to the language model RoBERTa [17] and utilize the GLUE benchmark [32] to assess the generalizability of our approach. Given the diverse evaluation metrics across tasks, we follow Lu et al. [18] and report normalized score in Table 3, which leverages the fine-tuned models as upper bounds on performance to assess the effectiveness of the merging model. Table 3 presents the performance of various training-free methods for merging RoBERTa models across eight GLUE benchmark tasks. Specifically, our approach notably attains the highest average performance score of 68.3% on RoBERTa-Base and 74.5% on RoBERTa-Large, marking substantial enhancements over the baseline methods. Compared to the most advanced merging baseline, our methodology manifests a notable improvement of 0.5% on RoBERTa-Base and a substantial 1.7% increment on RoBERTa-Large. These results highlight the superior generalization ability of our methods on language models. Moreover, similar to the ViT series of vision models, we observe that the performance of the merge method approaches that of the individually fine-tuned models as the size of the model increases.

4.5. Robustness Analysis

Robustness Analysis on Task Numbers. We evaluated the performance of the merging model on in-domain tasks with varying numbers of tasks and compared the proposed method with Task Arithmetic and Ties-Merging. Figure 3a shows the average accuracy of these methods across different numbers of merged tasks, with error bars representing the 95% confidence interval. For each setting with different task numbers, we randomly sampled 8 subsets from all tasks and computed the average accuracy of the merging model on these subsets. More experimental details can be found in the supplementary materials. From Figure 3a,



(a) Cosine similarity between task vectors on ViT-B/32



(b) Cosine similarity between task vectors on ViT-L/14

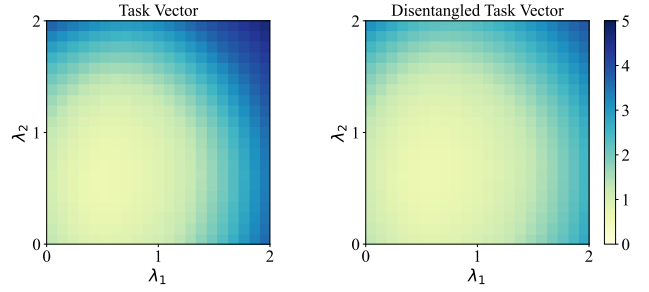
Figure 4. Cosine similarity heatmaps for task vectors and disentangled task vectors on ViT-B/32 and ViT-L/14.

the following conclusions can be drawn: (1) As the number of merged tasks increases, the performance of all methods shows a declining trend, indicating that increased task numbers lead to greater interference between tasks; (2) As the number of merged tasks increases, our method’s performance decreases more slowly compared to Task Arithmetic and Ties-Merging. Overall, task interference remains the primary factor affecting model performance. Compared to the other baseline methods, our approach significantly reduces interference between task vectors, demonstrating superior robustness when handling a larger number of tasks.

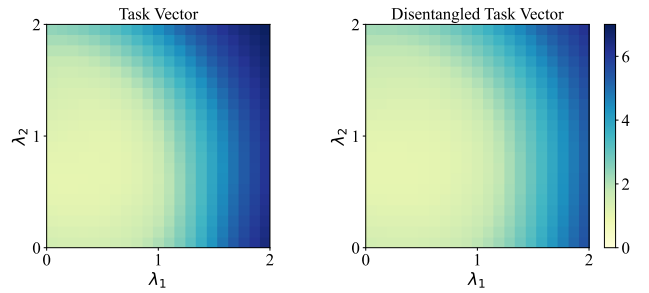
Robustness Analysis on Coefficients. In order to further assess the robustness of our method, we also conducted a comparative analysis of different coefficients for the merged task vectors. As shown in Figure 3b, we compared our approach with Task Arithmetic. From the results presented in the figure, it can be observed that when the coefficient is less than or equal to 0.2, our method performs similarly to Task Arithmetic; however, when the coefficient exceeds 0.2, our method significantly outperforms Task Arithmetic. This indicates that as the task vectors are scaled up, the interference between tasks is also amplified. Nonetheless, our method can effectively eliminate inter-task interference, making it more robust to changes in the coefficients.

4.6. Visualization Analysis

Similarity between Task Vectors. As shown in Figure 4, we measure the cosine similarity of the task vectors for the ViT-B/32 and ViT-L/14 models, respectively. Com-



(a) Loss landscape visualization on RESISC45 and Cars.



(b) Loss landscape visualization on SUN397 and DTD.

Figure 5. Loss landscape visualization. We visualize the loss landscape $\mathcal{L}_i(\hat{\Theta}) + \mathcal{L}_j(\hat{\Theta})$ by interpolating for ViT-B/32.

pared with original task vectors, our method significantly reduces the cosine similarity between task vectors of different tasks, which is crucial for reducing interference between tasks [10, 28]. We find that, for larger models, the cosine similarity between task vectors is smaller. This may also be the key to the differences in task arithmetic performance among models of different sizes shown in Tables 1 and 2.

Loss Landscape. To more clearly demonstrate the advantages of our AWD in reducing interference, we conducted a visualization analysis of the loss landscape for the joint tasks. Specifically, we performed interpolations on a 2D plane between the pre-trained model Θ and the task vectors, and separately between the pre-trained model and the disentangled task vectors. As depicted in Figure 5, the heatmaps represent the loss values $\mathcal{L}_i(\hat{\Theta}) + \mathcal{L}_j(\hat{\Theta})$ evaluated over the joint tasks. These figures show that the disentangled task vectors derived through our methodology exhibit a more expansive low-loss basin compared to the original task vector. This demonstrates that our approach effectively reduces interference between tasks. Moreover, as λ increases, regions initially shown in deep blue demonstrate a substantial reduction, indicating that our method is robust to variations in the coefficient λ , which is consistent with Section 4.5.

5. Conclusion

In this paper, we propose the task consistency property, which requires that a merged model’s performance on each task closely matches the performance achieved when only

the corresponding task vector is incorporated. In this context, task vectors satisfying this property are free from task interference. We theoretically demonstrate that this property can be approximately achieved by ensuring that task vectors are orthogonal. Based on this insight, we introduce Adaptive Weight Disentanglement, which decomposes traditional task vectors into a redundant vector and several disentangled task vectors, enhancing their orthogonality to approximate the solution of task consistency property. Experimental results show that our approach effectively reduces interference between tasks and significantly improves the performance of existing merging techniques.

References

- [1] Samuel Ainsworth, Jonathan Hayase, and Siddhartha Srinivasa. Git re-basin: Merging models modulo permutation symmetries. In *Proceedings of the Eleventh International Conference on Learning Representations*, 2023. 2
- [2] Rishabh Bhardwaj, Duc Anh Do, and Soujanya Poria. Language models are Homer simpson! safety re-alignment of fine-tuned language models through task arithmetic. In *Proceedings of the 62nd Annual Meeting of the Association for Computational Linguistics (Volume 1: Long Papers)*, pages 14138–14149, 2024. 2
- [3] Gong Cheng, Junwei Han, and Xiaoqiang Lu. Remote sensing image scene classification: Benchmark and state of the art. *Proceedings of the IEEE*, 105(10):1865–1883, 2017. 5, 13
- [4] Mircea Cimpoi, Subhransu Maji, Iasonas Kokkinos, Sammy Mohamed, and Andrea Vedaldi. Describing textures in the wild. In *Proceedings of the IEEE/CVF Conference on Computer Vision and Pattern Recognition*, pages 3606–3613, 2014. 5, 13
- [5] Damai Dai, Li Dong, Yaru Hao, Zhifang Sui, Baobao Chang, and Furu Wei. Knowledge neurons in pretrained transformers. In *Proceedings of the 60th Annual Meeting of the Association for Computational Linguistics (Volume 1: Long Papers)*, pages 8493–8502. Association for Computational Linguistics, 2022. 6
- [6] Mehrdad Farajtabar, Navid Azizan, Alex Mott, and Ang Li. Orthogonal gradient descent for continual learning. In *International Conference on Artificial Intelligence and Statistics*, pages 3762–3773. PMLR, 2020. 2
- [7] Yiduo Guo, Wenpeng Hu, Dongyan Zhao, and Bing Liu. Adaptive orthogonal projection for batch and online continual learning. *Proceedings of the AAAI Conference on Artificial Intelligence*, 36(6):6783–6791, 2022. 2
- [8] Yifei He, Yuzheng Hu, Yong Lin, Tong Zhang, and Han Zhao. Localize-and-stitch: Efficient model merging via sparse task arithmetic. 2024. 2
- [9] Patrick Helber, Benjamin Bischke, Andreas Dengel, and Damian Borth. Eurosat: A novel dataset and deep learning benchmark for land use and land cover classification. *IEEE Journal of Selected Topics in Applied Earth Observations and Remote Sensing*, 12(7):2217–2226, 2019. 5, 13
- [10] Gabriel Ilharco, Marco Tulio Ribeiro, Mitchell Wortsman, Ludwig Schmidt, Hannaneh Hajishirzi, and Ali Farhadi. Editing models with task arithmetic. In *Proceedings of the Eleventh International Conference on Learning Representations*, 2023. 1, 2, 3, 4, 5, 6, 8, 13, 14, 15
- [11] Xisen Jin, Xiang Ren, Daniel Preotiuc-Pietro, and Pengxiang Cheng. Dataless knowledge fusion by merging weights of language models. In *Proceedings of the Eleventh International Conference on Learning Representations*, 2023. 3, 6, 14
- [12] Keller Jordan, Hanie Sedghi, Olga Saukh, Rahim Entezari, and Behnam Neyshabur. REPAIR: RENormalizing permuted activations for interpolation repair. In *Proceedings of the Eleventh International Conference on Learning Representations*, 2023. 2
- [13] Jonathan Krause, Michael Stark, Jia Deng, and Li Fei-Fei. 3d object representations for fine-grained categorization. In *ICCV workshops*, pages 554–561, 2013. 5, 13
- [14] Yann LeCun. The mnist database of handwritten digits. <http://yann.lecun.com/exdb/mnist/>, 1998. 5, 13
- [15] Depeng Li, Tianqi Wang, Junwei Chen, Qining Ren, Kenji Kawaguchi, and Zhigang Zeng. Towards continual learning desiderata via hsic-bottleneck orthogonalization and equiangular embedding. *Proceedings of the AAAI Conference on Artificial Intelligence*, 38(12):13464–13473, 2024. 2
- [16] Jian Liang, Ziqi Liu, Jiayu Zhou, Xiaoqian Jiang, Changshui Zhang, and Fei Wang. Model-protected multi-task learning. *IEEE Transactions on Pattern Analysis and Machine Intelligence*, 44(2):1002–1019, 2022. 1
- [17] Yinhan Liu, Myle Ott, Naman Goyal, Jingfei Du, Mandar Joshi, Danqi Chen, Omer Levy, Mike Lewis, Luke Zettlemoyer, and Veselin Stoyanov. Roberta: A robustly optimized bert pretraining approach. 2019. 7
- [18] Zhenyi Lu, Chenghao Fan, Wei Wei, Xiaoye Qu, Danyang Chen, and Yu Cheng. Twin-merging: Dynamic integration of modular expertise in model merging. 2024. 7, 15, 16
- [19] Michael S Matena and Colin A Raffel. Merging models with fisher-weighted averaging. In *Proceedings of the International Conference on Neural Information Processing Systems*, pages 17703–17716, 2022. 3, 6, 14
- [20] Mohammed Muqeeth, Haokun Liu, Yufan Liu, and Colin Raffel. Learning to route among specialized experts for zero-shot generalization. In *Proceedings of the International Conference on Machine Learning*, 2024. 1
- [21] Guillermo Ortiz-Jimenez, Alessandro Favero, and Pascal Frossard. Task arithmetic in the tangent space: Improved editing of pre-trained models. In *Proceedings of the Conference on Neural Information Processing Systems*, 2023. 1, 2, 3, 12
- [22] Alec Radford, Jong Wook Kim, Chris Hallacy, Aditya Ramesh, Gabriel Goh, Sandhini Agarwal, Girish Sastry, Amanda Askell, Pamela Mishkin, Jack Clark, Gretchen Krueger, and Ilya Sutskever. Learning transferable visual models from natural language supervision. 2021. 1, 5, 15
- [23] Colin Raffel, Noam Shazeer, Adam Roberts, Katherine Lee, Sharan Narang, Michael Matena, Yanqi Zhou, Wei Li, and Peter J. Liu. Exploring the limits of transfer learning with a

- unified text-to-text transformer. *Journal of Machine Learning Research*, 21(1), 2020. 1
- [24] Gobinda Saha and Kaushik Roy. Continual learning with scaled gradient projection. In *Proceedings of the AAAI Conference on Artificial Intelligence*, pages 9677–9685, 2023. 2
- [25] Victor Sanh, Albert Webson, Colin Raffel, Stephen Bach, Lintang Sutawika, Zaid Alyafeai, Antoine Chaffin, Arnaud Stiegler, Arun Raja, Manan Dey, M Saiful Bari, Canwen Xu, Urmish Thakker, Shanya Sharma Sharma, Eliza Szczechla, Taewoon Kim, Gunjan Chhablani, Nihal Nayak, Debajyoti Datta, Jonathan Chang, Mike Tian-Jian Jiang, Han Wang, Matteo Manica, Sheng Shen, Zheng Xin Yong, Harshit Pandey, Rachel Bawden, Thomas Wang, Trishala Neeraj, Jos Rozen, Abheesht Sharma, Andrea Santilli, Thibault Fevry, Jason Alan Fries, Ryan Teehan, Teven Le Scao, Stella Biderman, Leo Gao, Thomas Wolf, and Alexander M Rush. Multitask prompted training enables zero-shot task generalization. In *Proceedings of the International Conference on Learning Representations*, 2022. 1
- [26] Johannes Stalldkamp, Marc Schlipfing, Jan Salmen, and Christian Igel. The german traffic sign recognition benchmark: a multi-class classification competition. In *International Joint Conference on Neural Networks*, pages 1453–1460. IEEE, 2011. 5, 13
- [27] Anke Tang, Li Shen, Yong Luo, Yibing Zhan, Han Hu, Bo Du, Yixin Chen, and Dacheng Tao. Parameter-efficient multi-task model fusion with partial linearization. In *Proceedings of the Twelfth International Conference on Learning Representations*, 2024. 2, 4
- [28] Anke Tang, Li Shen, Yong Luo, Yibing Zhan, Han Hu, Bo Du, Yixin Chen, and Dacheng Tao. Parameter-efficient multi-task model fusion with partial linearization. In *Proceedings of the Twelfth International Conference on Learning Representations*, 2024. 2, 8
- [29] Yi Tay, Mostafa Dehghani, Vinh Q. Tran, Xavier Garcia, Jason Wei, Xuezhi Wang, Hyung Won Chung, Dara Bahri, Tal Schuster, Steven Zheng, Denny Zhou, Neil Houlsby, and Donald Metzler. UL2: Unifying language learning paradigms. In *Proceedings of the Eleventh International Conference on Learning Representations*, 2023. 1
- [30] Rheeya Uppaal, Junjie Hu, and Yixuan Li. Is fine-tuning needed? pre-trained language models are near perfect for out-of-domain detection. In *Proceedings of the 61st Annual Meeting of the Association for Computational Linguistics (Volume 1: Long Papers)*, pages 12813–12832. Association for Computational Linguistics, 2023. 1
- [31] Fanqi Wan, Xinting Huang, Deng Cai, Xiaojun Quan, Wei Bi, and Shuming Shi. Knowledge fusion of large language models. In *Proceedings of the Twelfth International Conference on Learning Representations*, 2024. 2
- [32] Alex Wang, Amanpreet Singh, Julian Michael, Felix Hill, Omer Levy, and Samuel Bowman. GLUE: A multi-task benchmark and analysis platform for natural language understanding. In *Proceedings of the 2018 EMNLP Workshop BlackboxNLP: Analyzing and Interpreting Neural Networks for NLP*, pages 353–355, 2018. 7
- [33] Ke Wang, Nikolaos Dimitriadis, Guillermo Ortiz-Jimenez, François Fleuret, and Pascal Frossard. Localizing task information for improved model merging and compression. In *Proceedings of the 41st International Conference on Machine Learning*, pages 50268–50287. PMLR, 2024. 2, 3, 6, 14
- [34] Liyuan Wang, Xingxing Zhang, Hang Su, and Jun Zhu. A comprehensive survey of continual learning: Theory, method and application. *IEEE Transactions on Pattern Analysis and Machine Intelligence*, 46(8):5362–5383, 2024. 2
- [35] Xiao Wang, Tianze Chen, Qiming Ge, Han Xia, Rong Bao, Rui Zheng, Qi Zhang, Tao Gui, and Xuanjing Huang. Orthogonal subspace learning for language model continual learning. *arXiv preprint arXiv:2310.14152*, 2023. 2
- [36] Mitchell Wortsman, Gabriel Ilharco, Samir Ya Gadre, Rebecca Roelofs, Raphael Gontijo-Lopes, Ari S Morcos, Hongseok Namkoong, Ali Farhadi, Yair Carmon, Simon Kornblith, and Ludwig Schmidt. Model soups: averaging weights of multiple fine-tuned models improves accuracy without increasing inference time. In *Proceedings of the 39th International Conference on Machine Learning*, pages 23965–23998. PMLR, 2022. 3, 6
- [37] Jianxiong Xiao, Krista A Ehinger, James Hays, Antonio Torralba, and Aude Oliva. Sun database: Exploring a large collection of scene categories. *International Journal of Computer Vision*, 119:3–22, 2016. 5, 13
- [38] Yichen Xie, Han Lu, Junchi Yan, Xiaokang Yang, Masayoshi Tomizuka, and Wei Zhan. Active finetuning: Exploiting annotation budget in the pretraining-finetuning paradigm. In *Proceedings of the IEEE/CVF Conference on Computer Vision and Pattern Recognition*, pages 23715–23724, 2023. 1
- [39] Prateek Yadav, Derek Tam, Leshem Choshen, Colin Raffel, and Mohit Bansal. Ties-merging: resolving interference when merging models. In *Proceedings of the International Conference on Neural Information Processing Systems*, pages 7093–7115, 2023. 1, 2, 3, 4, 5, 6, 12, 13, 14
- [40] Enneng Yang, Li Shen, Guibing Guo, Xingwei Wang, Xiaochun Cao, Jie Zhang, and Dacheng Tao. Model merging in llms, mllms, and beyond: Methods, theories, applications and opportunities. 2024. 1, 2
- [41] Enneng Yang, Li Shen, Zhenyi Wang, Guibing Guo, Xiaojun Chen, Xingwei Wang, and Dacheng Tao. Representation surgery for multi-task model merging. In *Proceedings of the 41st International Conference on Machine Learning*, pages 56332–56356. PMLR, 2024. 5, 6, 14
- [42] Enneng Yang, Zhenyi Wang, Li Shen, Shiwei Liu, Guibing Guo, Xingwei Wang, and Dacheng Tao. Adamerging: Adaptive model merging for multi-task learning. In *Proceedings of the Twelfth International Conference on Learning Representations*, 2024. 2, 5, 6, 13, 14
- [43] Zi Yin and Yuanyuan Shen. On the dimensionality of word embedding. In *Proceedings of the International Conference on Neural Information Processing Systems*. Curran Associates, Inc., 2018. 6
- [44] Le Yu, Bowen Yu, Haiyang Yu, Fei Huang, and Yongbin Li. Language models are super mario: Absorbing abilities from homologous models as a free lunch. In *Proceedings of the International Conference on Machine Learning*. PMLR, 2024. 2, 3, 4, 5, 12

- [45] Netzer Yuval. Reading digits in natural images with unsupervised feature learning. In *NIPS Workshop on Deep Learning and Unsupervised Feature Learning*, 2011. [5](#), [13](#)
- [46] Guanxiong Zeng, Yang Chen, Bo Cui, and Shan Yu. Continual learning of context-dependent processing in neural networks. *Nature Machine Intelligence*, 1(8):364–372, 2019. [2](#)

Multi-Task Model Merging via Adaptive Weight Disentanglement

Supplementary Material

6. Further Theoretical Derivation

6.1. Analysis of Invariance Optimization Objective

Inspired by previous works [39, 44], we empirically incorporate the norm of δ as **Invariance** objective to ensure that each disentangled task vector performs well on its corresponding specific task. Herein, we further engage in a theoretical examination of the rationality of this optimization objective. Ideally, we aim for each disentangled task vector to individually preserve the performance of the original task vector on its corresponding specific task. We define the **Replacement Gap** \mathcal{R}_i as the discrepancy in performance between the disentangled task vector $\hat{\tau}_i$ and the original task vector τ_i on a specific task i . Then, \mathcal{R}_i can be described as,

$$\mathcal{R}_i = \mathcal{L}_i(\Theta + \hat{\tau}_i) - \mathcal{L}_i(\Theta + \tau_i). \quad (15)$$

We apply the Taylor expansion to $\mathcal{L}_i(\Theta + \hat{\tau}_i)$ and $\mathcal{L}_i(\Theta + \tau_i)$. Taking $\mathcal{L}_i(\Theta + \hat{\tau}_i)$ as an example,

$$\mathcal{L}_i(\Theta + \hat{\tau}_i) \approx \mathcal{L}_i(\Theta) + \langle \nabla_{\Theta} \mathcal{L}_i(\Theta), \hat{\tau}_i \rangle + \frac{1}{2} \hat{\tau}_i^{\top} \mathbf{H}_i \hat{\tau}_i, \quad (16)$$

where \mathbf{H}_i is the Hessian of the loss \mathcal{L}_i at Θ . Given that τ_i is generally negligible [44], the second-order terms can typically be approximated as zero. As a result, Equation 15 can be simplified accordingly.

$$\begin{aligned} \mathcal{R}_i &\approx \mathcal{L}_i(\Theta) + \langle \nabla_{\Theta} \mathcal{L}_i(\Theta), \hat{\tau}_i \rangle - \mathcal{L}_i(\Theta) - \langle \nabla_{\Theta} \mathcal{L}_i(\Theta), \tau_i \rangle \\ &= \langle \nabla_{\Theta} \mathcal{L}_i(\Theta), \hat{\tau}_i - \tau_i \rangle \end{aligned} \quad (17)$$

$$= \langle \nabla_{\Theta} \mathcal{L}_i(\Theta), \tau_i - \delta - \tau_i \rangle \quad (18)$$

$$= \langle \nabla_{\Theta} \mathcal{L}_i(\Theta), -\delta \rangle \quad (19)$$

$$= |\nabla_{\Theta} \mathcal{L}_i(\Theta)| \cos(\nabla_{\Theta} \mathcal{L}_i(\Theta), -\delta) \quad (20)$$

$$\leq \underbrace{|\nabla_{\Theta} \mathcal{L}_i(\Theta)|}_{\text{Fixed Value}} \underbrace{\|\delta\|}_{\text{Redundant Vector Norm}} \quad (21)$$

$$\leq \underbrace{|\nabla_{\Theta} \mathcal{L}_i(\Theta)|}_{\text{Fixed Value}} \underbrace{\|\delta\|}_{\text{Redundant Vector Norm}} \quad (22)$$

From Eq. 22, when we incorporate the norm of δ into the optimization objective, it optimizes the upper bound of the Replacement Gap \mathcal{R}_i . This is beneficial for the disentangled task vectors to closely approximate the performance of the original task vectors on their respective specific tasks.

6.2. Solutions for Task Consistency Property

In our paper, we define Task Consistency Property as the performance of the merged multi-task model on each individual task should approximate the performance obtained

when only the corresponding task vector is integrated. This definition serves as a natural extension of Task Arithmetic Property [21], aligning more closely with the objectives of multi-task model merging and presenting a more tractable solution. The formal expression is as follows:

Task Consistency Property. *Given coefficient sets $\{\lambda_i\}_{i=1}^K \subset \mathbb{R}$ and a set of task vectors $\mathcal{T} = \{\tau_i\}_{i=1}^K$ correspond with non-intersecting task-specific data supports $\mathcal{D} = \{\mathcal{D}_i\}_{i \in [K]}$, i.e., $\forall t, t', \text{ if } t \neq t' \text{ then } \mathcal{D}_t \cap \mathcal{D}_{t'} = \emptyset$. We say a network f satisfies the task consistency property around Θ with respect to \mathcal{T} and \mathcal{D} if:*

$$\forall \mathcal{D}_i \in \mathcal{D}, \mathcal{L}_i \left(\Theta + \sum_j^K \lambda_j \tau_j \right) = \mathcal{L}_i(\Theta + \lambda_i \tau_i), \quad (23)$$

where $\mathcal{L}_i(\cdot)$ denotes the loss function of task i . We fix the pre-trained model and solve for the task vector that satisfies task consistency property, which guides us in refining the task vector. To simplified the Eq. 2, we define the **Merging Gap** G_i as,

$$G_i = \mathcal{L}_i \left(\Theta + \sum_j^K \lambda_j \tau_j \right) - \mathcal{L}_i(\Theta + \lambda_i \tau_i). \quad (24)$$

Based on the aforementioned formulation, the task consistency property can be reformulated as follows,

$$\forall i, G_i = 0. \quad (25)$$

We apply Tylor expansion to $\mathcal{L}_i \left(\Theta + \sum_j^K \lambda_j \tau_j \right)$ and $\mathcal{L}_i(\Theta + \lambda_i \tau_i)$ around Θ . We take $\mathcal{L}_i \left(\Theta + \sum_j^K \lambda_j \tau_j \right)$ as an instance, it can be approximated as:

$$\mathcal{L}_i \left(\Theta + \sum_j^K \lambda_j \tau_j \right) \approx \mathcal{L}_i(\Theta) + \left\langle \nabla_{\Theta} \mathcal{L}_i(\Theta), \sum_j^K \lambda_j \tau_j \right\rangle \quad (26)$$

$$+ \frac{1}{2} \left(\sum_j^K \lambda_j \tau_j \right)^{\top} \mathbf{H}_i \left(\sum_j^K \lambda_j \tau_j \right), \quad (27)$$

where \mathbf{H}_i is the Hessian of the loss \mathcal{L}_i at Θ . Given that λ_j typically falls within the range of $(-1, 1)$ and τ_j is generally quite small [44], the second-order terms can generally be approximated as zero under standard conditions. Eq. 24 can

be simplified as,

$$G_i = \mathcal{L}_i \left(\Theta + \sum_j^K \lambda_j \tau_j \right) - \mathcal{L}_i (\Theta + \lambda_i \tau_i) \quad (28)$$

$$\approx \left(\mathcal{L}_i (\Theta) + \left\langle \nabla_{\Theta} \mathcal{L}_i (\Theta), \sum_j^K \lambda_j \tau_j \right\rangle \right) \quad (29)$$

$$- (\mathcal{L}_i (\Theta) + \langle \nabla_{\Theta} \mathcal{L}_i (\Theta), \lambda_i \tau_i \rangle) \quad (30)$$

$$= \left\langle \nabla_{\Theta} \mathcal{L}_i (\Theta), \sum_j^K \lambda_j \tau_j \right\rangle - \langle \nabla_{\Theta} \mathcal{L}_i (\Theta), \lambda_i \tau_i \rangle \quad (31)$$

$$= \left\langle \nabla_{\Theta} \mathcal{L}_i (\Theta), \lambda_i \tau_i + \sum_{j \neq i}^K \lambda_j \tau_j \right\rangle - \langle \nabla_{\Theta} \mathcal{L}_i (\Theta), \lambda_i \tau_i \rangle \quad (32)$$

$$= \left\langle \nabla_{\Theta} \mathcal{L}_i (\Theta), \sum_{j \neq i}^K \lambda_j \tau_j \right\rangle \quad (33)$$

$$= \sum_{j \neq i}^K \langle \nabla_{\Theta} \mathcal{L}_i (\Theta), \lambda_j \tau_j \rangle. \quad (34)$$

Obtaining the original data for gradient calculation in a pre-trained model for a specific task can often be challenging due to accessibility issues. An effective alternative is to substitute this gradient with the task vector, as the task vector can be conceptualized as the accumulation of gradients. Therefore, Eq. 24 can be described as,

$$G_i = \sum_{j \neq i}^K \langle k_i \tau_i, \lambda_j \tau_j \rangle \quad (35)$$

$$= k_i \sum_{j \neq i}^K \langle \tau_i, \lambda_j \tau_j \rangle, \quad (36)$$

where $k_i < 0$. Since λ_j is typically a hyperparameter, directly solving the previously mentioned equation is challenging. Consequently, our objective is to identify a specific solution for this equation. As demonstrated in Eq. 36, Eq. 2 will be satisfied when all task vectors are orthogonal to each other,

$$\forall i \neq j, \cos(\tau_i, \tau_j) = 0 \Rightarrow \forall i, G_i = 0. \quad (37)$$

7. Experimental Settings

This section offers comprehensive descriptions of the datasets, baselines, and implementations.

7.1. Datasets Details

Following Task Arithmetic [10], Ties-Merging [39], and AdaMerging [42], our research employs eight image classification benchmarks to assess the efficacy of multi-task model merging. The datasets can be detailed as follows.

- **SUN397** [37] is a scene classification dataset, containing 108,753 images of 397 categories, with each category containing at least 100 images.
- **Cars** [13] is a specialized resource for fine-grained vehicle recognition, comprising 16,185 images across 196 distinct classes of cars. The dataset is evenly divided into 8,144 training images and 8,041 testing images.
- **RESISC45** [3] is designed for Remote Sensing Image Scene Classification and comprises 31,500 images. It is categorized into 45 distinct scene classes, with each class uniformly represented by 700 images.
- **EuroSAT** [9] serves as a benchmark for land use and land cover classification, featuring 27,000 labeled and geo-referenced images derived from Sentinel-2 satellite imagery. This dataset encompasses 13 spectral bands and is organized into 10 distinct classes.
- **SVHN** [45] is a digit classification dataset extracted from house numbers depicted in Google Street View images. SVHN includes 10 classes and is partitioned into a training set comprising 73,257 images, a test set containing 26,032 images, and an additional set of 531,131 images that can be utilized for extended training purposes.
- **GTSRB** [26] is focusing on traffic sign recognition. This dataset comprises a total of 51,839 images, which are categorized into 43 distinct classes of traffic signs. It is divided into a training set containing 39,209 images and a test set consisting of 12,630 images.
- **MNIST** [14] is a widely-used benchmark for handwritten digit recognition, consisting of a training set of 60,000 examples and a test set of 10,000 examples.
- **DTD** [4] is a comprehensive collection of natural texture images, amassing a total of 5640 images. These images are categorized into 47 distinct classes with each class comprising 120 images.

7.2. Baseline Details

We categorize the baselines into three main groups: Non-merging methods, Training-free methods, and Test-time Adaptation methods.

Non-merging Methods:

- **Pretrained** employs pre-trained models for each task without integrating task-specific information, thereby serving as a fundamental benchmark.
- **Individual** utilizes models that have been fine-tuned specifically for each task. In this context, there is no interference between tasks.
- **Traditional MTL** involves joint training using training data from multiple tasks. This approach necessitates access to the original data and poses challenges in scaling to new tasks.

Training-free Methods:

- **Weight Averaging** is the most straightforward approach to model merging, achieved by directly averaging the pa-

Table 4. Multi-task performance when merging ViT-B/16 models on eight tasks. The best performance across different merging methods is denoted in bold.

| Method | SUN397 | Cars | RESISC45 | EuroSAT | SVHN | GTSRB | MNIST | DTD | Avg Acc |
|-----------------------------------|-------------|-------------|-------------|-------------|-------------|-------------|-------------|-------------|-------------|
| <i>Non-merging Methods</i> | | | | | | | | | |
| Pretrained | 63.8 | 64.6 | 65.7 | 54.5 | 52.0 | 43.3 | 51.7 | 45.1 | 55.0 |
| Individual | 81.8 | 86.8 | 96.9 | 99.7 | 97.8 | 99.1 | 99.7 | 82.0 | 92.9 |
| <i>Training-free Methods</i> | | | | | | | | | |
| Weight Averaging | 67.7 | 70.0 | 75.3 | 79.5 | 74.9 | 60.1 | 94.4 | 43.8 | 70.7 |
| Fisher Merging | 68.5 | 69.9 | 75.2 | 80.4 | 73.2 | 61.2 | 94.5 | 50.7 | 71.7 |
| RegMean | 69.1 | 71.6 | 77.6 | 88.8 | 83.7 | 70.2 | 96.9 | 54.6 | 76.6 |
| Task Arithmetic | 61.1 | 65.9 | 74.0 | 76.2 | 88.0 | 73.9 | 98.4 | 53.0 | 73.8 |
| Ties-Merging | 69.1 | 72.5 | 80.5 | 84.0 | 85.0 | 71.5 | 98.1 | 54.9 | 77.0 |
| Consensus Merging | 69.8 | 71.4 | 80.8 | 86.5 | 88.0 | 71.1 | 98.4 | 57.0 | 77.9 |
| AWD Task Arithmetic (Ours) | 67.8 | 72.7 | 78.7 | 88.5 | 90.9 | 83.6 | 98.9 | 57.1 | 79.8 |
| <i>Test-time Adaption Methods</i> | | | | | | | | | |
| TW AdaMerging | 64.4 | 64.2 | 75.4 | 86.7 | 86.3 | 86.7 | 97.6 | 46.9 | 76.0 |
| LW AdaMerging | 70.2 | 80.7 | 81.6 | 94.8 | 91.6 | 95.8 | 98.5 | 66.2 | 84.9 |
| Representation Surgery | 68.3 | 72.3 | 88.7 | 97.7 | 91.0 | 89.5 | 98.9 | 72.9 | 84.9 |
| AWD AdaMerging (Ours) | 71.5 | 81.9 | 84.3 | 94.6 | 93.3 | 96.8 | 98.6 | 72.6 | 86.7 |

rameters of several models.

- **Fisher Merging** [19] utilizes the Fisher information matrix to evaluate the significance of each parameter, guiding the merging process based on this assessment.
- **RegMean** [11] aims to minimize the predictive differences between the merged model and the individual task-specific models.
- **Task Arithmetic** [10] introduces the concept of task vectors and achieves model merging by performing arithmetic operations on these task vectors, integrating them into a pre-trained model to facilitate multi-task learning.
- **Ties-Merging** [39] mitigates task interference by eliminating redundant parameters, resolving sign conflicts, and averaging parameters that are consistent with the dominant direction.
- **Consensus Merging** [33] improves the effectiveness of existing model merging techniques by removing selfish and catastrophic weights, which are important exclusively to individual task and irrelevant to the other tasks but detrimental to model merging.

Test-time Adaption Methods:

- **TW AdaMerging** [42] employs entropy optimization to determine the merging coefficients for task vectors by leveraging an unlabeled test set.
- **LW AdaMerging** [42] adopts entropy optimization to independently deduce the merging coefficients for individual layers of task vectors.
- **TW AdaMerging++** [42] implements entropy optimization to identify the merging coefficients for task vectors in Ties-Merging autonomously.
- **LW AdaMerging++** [42] applies entropy optimization to compute the merging coefficients for each layer of task

vectors in Ties-Merging.

- **Representation Surgery** [41] addresses the issue of representation bias by employing an unsupervised optimization objective that minimizes the distance between the representations of the merged model and those of the individual models. In our work, we use Surgery integrated with Task Arithmetic as the baseline.

Table 5. Computational time and GPU memory requirements for solving redundant vector across eight vision tasks over 1000 solution steps were assessed on NVIDIA A100 40GB.

| Model | Solving Time | GPU Memory |
|----------|--------------|------------|
| ViT-B/32 | 2min22s | 3.76GB |
| ViT-L/14 | 7min43s | 5.04GB |

7.3. Implementation Details

Calculate Resources and Environment. All of our experiments were conducted on NVIDIA A100 40GB and NVIDIA H100 80GB. Due to the specific configuration of AdaMerging, we used the NVIDIA H100 80GB for the ViT-L/14 variant, while other experiments were conducted on the NVIDIA A100 40GB. The software environment for our experiments comprised Python 3.10, PyTorch 2.4.0, and the CUDA 11.8 toolkit. As illustrated in Table 5, our methodology incurs minimal computational overhead across different model versions, demonstrating near-universal scalability on devices equipped with contemporary GPUs.

Checkpoints for Merging. For the vision models, the checkpoints we utilized are sourced from Ilharco et al. [10],

Table 6. Multi-task performance when merging ViT-B/32 models on 8-task vision benchmark, where Individual Reconstructed refers to task-specific models that are reconstructed by combining disentangled task vectors with the pre-trained model respectively. By utilizing the orthogonality optimization objective, we can derive disentangled task vectors with increased orthogonality. Conversely, by employing a reverse optimization objective, we can obtain disentangled task vectors with decreased orthogonality.

| Method | SUN397 | Cars | RESISC45 | EuroSAT | SVHN | GTSRB | MNIST | DTD | Avg Acc |
|-------------------------------------------|--------|------|----------|---------|------|-------|-------|------|---------|
| Pretrained | 62.3 | 59.7 | 60.7 | 45.5 | 31.4 | 32.6 | 48.5 | 43.8 | 48.0 |
| Individual | 79.2 | 77.7 | 96.1 | 99.7 | 97.5 | 98.7 | 99.7 | 79.4 | 90.8 |
| Task Arithmetic | 55.2 | 54.9 | 66.7 | 78.9 | 80.2 | 69.7 | 97.3 | 50.4 | 69.1 |
| <i>Increased Orthogonality (Ours)</i> | | | | | | | | | |
| Individual Reconstructed | 79.3 | 77.6 | 96.1 | 99.8 | 97.4 | 98.8 | 99.7 | 78.8 | 90.9 |
| AWD Task Arithmetic | 63.5 | 61.9 | 72.6 | 84.9 | 85.1 | 79.1 | 98.1 | 56.7 | 75.2 |
| <i>Decreased Orthogonality (Reversed)</i> | | | | | | | | | |
| Individual Reconstructed | 78.3 | 76.6 | 95.6 | 99.6 | 97.4 | 98.8 | 99.7 | 78.6 | 90.6 |
| AWD Task Arithmetic | 2.7 | 1.1 | 19.3 | 42.1 | 60.1 | 20.1 | 92.6 | 16.7 | 31.8 |

Table 7. Multi-task performance when merging ViT-L/14 models on 8-task vision benchmark, where Individual Reconstructed refers to task-specific models that are reconstructed by combining disentangled task vectors with the pre-trained model respectively.

| Method | SUN397 | Cars | RESISC45 | EuroSAT | SVHN | GTSRB | MNIST | DTD | Avg Acc |
|-------------------------------------------|--------|------|----------|---------|------|-------|-------|------|---------|
| Pretrained | 66.8 | 77.7 | 71.0 | 59.9 | 58.4 | 50.5 | 76.3 | 55.3 | 64.5 |
| Individual | 82.3 | 92.4 | 97.4 | 100 | 98.1 | 99.2 | 99.7 | 84.1 | 94.2 |
| Task Arithmetic | 73.9 | 82.1 | 86.6 | 94.1 | 87.9 | 86.7 | 98.9 | 65.6 | 84.5 |
| <i>Increased Orthogonality (Ours)</i> | | | | | | | | | |
| Individual Reconstructed | 84.8 | 92.4 | 97.3 | 99.7 | 98.1 | 99.3 | 99.7 | 84.3 | 94.4 |
| AWD Task Arithmetic | 76.2 | 85.4 | 88.7 | 96.1 | 92.4 | 92.3 | 99.3 | 69.4 | 87.5 |
| <i>Decreased Orthogonality (Reversed)</i> | | | | | | | | | |
| Individual Reconstructed | 84.6 | 92.3 | 97.4 | 99.7 | 98.2 | 99.3 | 99.7 | 84.4 | 94.4 |
| AWD Task Arithmetic | 36.0 | 31.5 | 48.5 | 54.9 | 83.2 | 54.3 | 97.6 | 37.9 | 55.5 |

which were obtained by fine-tuning the CLIP model [22] using the AdamW optimizer with a weight decay of 0.1. The parameters involved include a batch size of 128 and a learning rate of $1e-5$, employing a cosine annealing learning rate schedule over 2000 iterations, which includes 200 warm-up steps. For the language models, we utilize RoBERTa-Base and RoBERTa-Large as the pretrained backbones. Our checkpoints are derived from Lu et al. [18]. These checkpoints underwent 10 epochs of fine-tuning on the RoBERTa model for each dataset, with selected hyperparameters including a batch size of 64 and a learning rate of $1e-5$.

Hyper-parameter tuning. To balance the relationship between orthogonality and invariance, we tune the hyper-parameter Constraints Coefficient α over a range of $\{1e-2, 1e-3, 1e-4, 1e-5, 1e-6\}$. For AWD Task Arithmetic: We follow Ilharco et al. [10], and we use a single scaling factor λ to scale the sum of the disentangled task vectors for the model merging. The scaling factor λ is tuned over a range of $\{0.3, 0.4, \dots, 1.0\}$. For AWD AdaMerging: we use 0.3 or 0.4 to initialize each λ_{ij} . The best α and λ are selected based on the performance of the validation set averaged on all tasks.

8. Additional Experimentals

8.1. Performance on ViT-B/16

Table 4 presents the performance of various merging methods applied to ViT-B/16. Our approach achieves a 6.0% improvement over Task Arithmetic and a 1.8% gain compared to AdaMerging on corresponding settings. These results strongly indicate that our method effectively mitigates conflicts between task vectors, further demonstrating the effectiveness of our AWD in multi-task model merging.

8.2. More Discussions on Orthogonality

To further validate the effectiveness of our approximate orthogonal solutions, we conducted a detailed analysis of the relationship between the cosine similarity between task vectors and the performance of the merged model. Given the fixed λ , by tuning the value of α , we ensured that the disentangled task vector could proficiently restore the performance of the specific task associated with the original task vector, concurrently adjusting the orthogonality among the disentangled task vectors.

Fig. 6a and Fig. 6b depict the correlation between nor-

Table 8. Multi-task performance when merging RoBERTa-Base models on 8-task GLUE benchmark. We report normalized score [18]. The best and second-best performing model combination methods for each task are indicated in bold and underlined, respectively.

| Method | CoLA | SST-2 | MRPC | STS-B | QQP | QNLI | MNLI | RTE | Avg |
|-----------------------------------|-------------|-------------|-------------|-------------|-------------|-------------|-------------|-------------|-------------|
| Pretrained | 0.0 | 53.8 | 85.0 | 4.0 | 37.5 | 53.1 | 37.1 | 71.2 | 41.7 |
| Individual | 100.0 | 100.0 | 100.0 | 100.0 | 100.0 | 100.0 | 100.0 | 100.0 | 100.0 |
| Weight Averaging | 0.0 | 59.2 | 85.8 | 47.0 | 45.4 | 63.9 | 48.0 | 71.2 | 52.6 |
| Task Arithmetic | 8.4 | 88.3 | 89.6 | 32.8 | 82.0 | 85.4 | 75.5 | <u>80.4</u> | <u>67.8</u> |
| Ties-Merging | 31.8 | <u>88.9</u> | 86.2 | 10.9 | 61.1 | <u>85.9</u> | <u>83.0</u> | 69.6 | 64.7 |
| Task Arithmetic (w/ DARE) | 0.0 | 88.1 | 86.6 | 30.2 | <u>84.3</u> | 79.1 | 64.0 | 77.2 | 63.7 |
| Ties-Merging (w/ DARE) | <u>11.8</u> | 95.5 | 85.8 | 9.4 | 86.8 | 88.7 | 83.1 | 63.6 | 65.6 |
| AWD Task Arithmetic (Ours) | <u>11.8</u> | 88.3 | <u>89.1</u> | <u>33.2</u> | 80.8 | 85.7 | 76.1 | 81.5 | 68.3 |

Table 9. Multi-task performance when merging RoBERTa-Large models on 8-task GLUE benchmark. We report normalized score [18]. The best and second-best performing model combination methods for each task are indicated in bold and underlined, respectively.

| Method | CoLA | SST-2 | MRPC | STS-B | QQP | QNLI | MNLI | RTE | Avg |
|-----------------------------------|-------------|-------------|-------------|-------------|-------------|-------------|-------------|-------------|-------------|
| Pre-trained | 0.0 | 51.5 | 40.9 | 20.9 | 36.4 | 56.0 | 37.6 | 62.4 | 38.2 |
| Individual | 100.0 | 100.0 | 100.0 | 100.0 | 100.0 | 100.0 | 100.0 | 100.0 | 100.0 |
| Weight Averaging | 7.4 | 55.1 | 84.2 | 46.3 | 56.7 | 73.8 | 35.8 | 66.7 | 53.3 |
| Task Arithmetic | 7.4 | 86.1 | 86.8 | <u>78.0</u> | 90.7 | 77.0 | 73.3 | 67.6 | 70.9 |
| Ties-Merging | 42.7 | 78.1 | 85.2 | 51.7 | 89.9 | 81.9 | 79.7 | 70.0 | 72.4 |
| Task Arithmetic (w/ DARE) | 4.1 | 85.2 | 85.8 | 71.6 | 91.3 | 85.6 | 75.2 | 68.1 | 70.9 |
| Ties-Merging (w/ DARE) | 2.9 | <u>90.4</u> | 86.8 | 75.4 | 92.4 | <u>86.4</u> | <u>79.0</u> | <u>69.1</u> | <u>72.8</u> |
| AWD Task Arithmetic (Ours) | <u>10.4</u> | 90.8 | <u>86.5</u> | 87.1 | <u>91.8</u> | 87.1 | 78.1 | 63.8 | 74.5 |

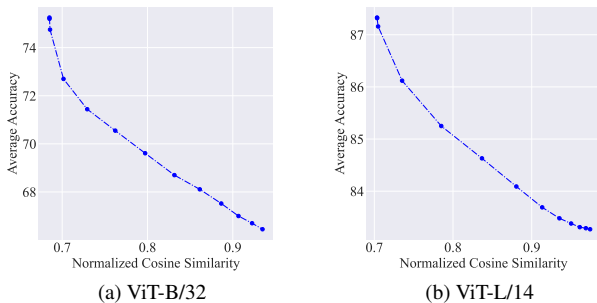


Figure 6. Correlation between normalized cosine similarity between disentangled task vectors and merged model performance. The normalized cosine score is calculated by normalizing the cosine similarity between the disentangled task vectors with respect to that of the original task vectors.

malized cosine similarity of the task vectors and the performance of the merged model on ViT-B/32 and ViT-L/14, respectively. We observe that as the normalized cosine similarity between disentangled task vectors decreases, the performance of the merged model correspondingly improves. Based on these findings, we can infer that enhancing the orthogonality among disentangled task vectors is beneficial in mitigating interference between them, thereby achieving a more effective fusion. This further bolsters our strategy of

considering the orthogonality of the disentangled task vectors as an optimization objective.

Furthermore, we investigate the impact of reducing orthogonality on model merging by reversing the orthogonality optimization objective, as shown in Table 6 and Table 7. Under different optimization objectives, we ensure that the disentangled task vectors can still recover the performance of the original task vectors. Compared to task arithmetic, by reversing the optimization objective, our AWD exhibits a performance decrease of 37.3% on ViT-B/32 and 29.0% on ViT-L/14. This implies that reducing the orthogonality among task vectors could intensify the interference between them, potentially undermining the model’s capacity for effective task integration.

8.3. Generalization in Language Models

Metrics: Following Lu et al. [18], we utilize the normalized scores as the assessment criterion. Similarly, we define the individually fine-tuned models as the upper performance bounds and the pre-trained models as the lower bounds. The Normalized Score is described as follows:

$$\text{Normalized Score} = \frac{1}{K} \sum_i^K \frac{\text{Score}[f(x; \hat{\Theta})]}{\text{Score}[f(x; \Theta_i^*)]} \quad (38)$$

Detailed Results: In the main paper, we demonstrated the effectiveness of our approach on the RoBERTa language

Table 10. Generalization results on two unseen tasks when merging ViT-B/16 models on six tasks.

| Method | Seen Tasks | | | | | | | Unseen Tasks | | |
|-----------------------------------|------------|------|----------|------|------|-------|---------|--------------|-------|---------|
| | SUN397 | Cars | RESISC45 | DTD | SVHN | GTSRB | Avg Acc | EuroSAT | MNIST | Avg Acc |
| Task Arithmetic | 68.1 | 73.0 | 81.6 | 59.1 | 89.1 | 83.8 | 75.8 | 43.9 | 87.5 | 65.7 |
| AWD Task Arithmetic (Ours) | 70.9 | 76.3 | 85.1 | 61.9 | 91.7 | 88.7 | 79.1 | 44.6 | 87.7 | 66.2 |

| Method | SUN397 | Cars | GTSRB | EuroSAT | DTD | MNIST | Avg Acc | RESISC45 | SVHN | Avg Acc |
|-----------------------------------|-----------------|------|-------|---------|------|-------|---------|----------|------|---------|
| | Task Arithmetic | 69.0 | 73.8 | 81.1 | 87.6 | 58.2 | 98.4 | 78.0 | 56.0 | 67.7 |
| AWD Task Arithmetic (Ours) | 72.3 | 77.0 | 85.4 | 93.5 | 76.7 | 98.5 | 81.1 | 58.2 | 68.6 | 63.4 |

Table 11. Comparison of performance across multiple task setups using various methods. Red text indicates the performance improvements compared to Task Arithmetic for each configuration.

| Method | 2-Tasks | 3-Tasks | 4-Tasks | 5-Tasks | 6-Tasks | 7-Tasks | 8-Tasks |
|-----------------------------------|-------------------|-------------------|-------------------|-------------------|-------------------|-------------------|-------------------|
| Individual | 93.0 | 90.6 | 92.5 | 90.1 | 91.5 | 91.4 | 90.6 |
| Task Arithmetic | 91.8 | 84.1 | 82.3 | 77.1 | 75.7 | 72.6 | 69.1 |
| Ties-Merging | 92.6 Δ 0.8 | 85.6 Δ 1.5 | 83.9 Δ 1.6 | 79.2 Δ 2.1 | 77.6 Δ 1.9 | 75.1 Δ 2.5 | 72.4 Δ 3.3 |
| AWD Task Arithmetic (Ours) | 92.4 Δ 0.6 | 85.7 Δ 1.6 | 85.1 Δ 2.8 | 80.6 Δ 3.5 | 79.7 Δ 4.0 | 77.1 Δ 4.5 | 75.2 Δ 6.1 |

models. As illustrated in Table 8 and Table 9, we further present detailed results of our method across various tasks.

8.4. Generalization on Unseen Tasks

As shown in Table 10, we conducted a comprehensive evaluation of AWD on both in-domain and out-of-domain tasks. Under the ViT-B/16 configuration, AWD demonstrated exceptional generalization performance. For in-domain tasks, our method achieved an average improvement of 3.3% across different settings. In cases where the corresponding task vectors were not merged (i.e., unseen tasks), our AWD method improved the average accuracy by 0.5% over the task arithmetic method on the EuroSAT and MNIST tasks; on the unseen tasks of RESISC45 and SVHN, the average accuracy was increased by 1.6%.

8.5. Empirical Upper Bound of AWD Task Arithmetic

For conventional training-free methods based on task vectors, there typically exists an adjustable coefficient λ . A disproportionately small λ may result in suboptimal performance of the task vector on its corresponding task, while an excessively large λ may amplify interference between tasks. Consequently, this coefficient plays a pivotal role in determining the performance of the merged model. According to Eq. 2, it can be seen that, the approximate upper bound of performance of our AWD Task Arithmetic on a specific task i can be represented as the performance of the integrated model $\Theta + \lambda\tau_i$. Here, $\Theta + \lambda\tau_i$ represents the amalgamation of the pretrained model with the individual task vector τ_i , which is proportionally scaled by λ . Therefore, we further conducted experiments on the performance under different λ coefficients. As shown in Fig. 7a and Fig. 7b, when

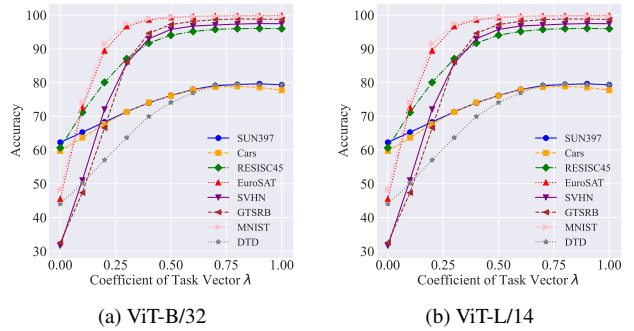


Figure 7. Performance of the integrated model $\Theta + \lambda\tau_i$ on corresponding task i across various values of λ . The integrated model $\Theta + \lambda\tau_i$ denotes as the combination of pre-trained models with individual task vector.

$\lambda > 0.3$ for each combination of $\Theta + \lambda\tau_i$, its performance is close to that of the fully fine-tuned model $\Theta_i^* = \Theta + \tau_i$. Moreover, as λ continues to increase, the rate of performance improvement sharply decreases. Notably, when λ is greater than 0.3, its performance has already surpassed the optimal merging method significantly. These results indicate that the approximate upper bound of our AWD Task Arithmetic is reasonable when $\lambda \geq 0.3$.

8.6. Performance across Different Task Numbers

In Table 11, we further evaluated our method across varying numbers of tasks. Specifically, when merging T tasks, there are a total of $\binom{8}{T}$ possible combinations. Therefore, in our experiment, we sampled 8 distinct combinations for each value of T and performed a hyperparameter search within the range $[0, 1]$ with a step size of 0.1 for each combination. It is evident that as the number of tasks increases, our

method demonstrates enhanced robustness against interference. For a more detailed analysis, please refer to Section 4.5 of the main paper.

The sampled task combinations are listed as follows:

- 2-Tasks: [[DTD, GTSRB], [GTSRB, SVHN], [GTSRB, SUN397], [SVHN, SUN397], [SVHN, GTSRB], [SVHN, EuroSAT], [SVHN, MNIST], [MNIST, Cars]]
- 3-Tasks: [[MNIST, SVHN, SUN397], [MNIST, SUN397, SVHN], [DTD, GTSRB, SUN397], [GTSRB, EuroSAT, Cars], [Cars, GTSRB, DTD], [MNIST, RESISC45, SVHN], [SVHN, MNIST, DTD], [RESISC45, SUN397, EuroSAT]]
- 4-Tasks: [EuroSAT, SVHN, Cars, SUN397], [MNIST, RESISC45, EuroSAT, GTSRB], [EuroSAT, Cars, RESISC45, MNIST], [DTD, SUN397, GTSRB, EuroSAT], [SUN397, EuroSAT, Cars, RESISC45], [RESISC45, MNIST, GTSRB, SUN397], [RESISC45, SVHN, GTSRB, MNIST], [SVHN, GTSRB, Cars, RESISC45]
- 5-Tasks: [[DTD, SVHN, GTSRB, SUN397, EuroSAT], [DTD, GTSRB, MNIST, RESISC45, SUN397], [SVHN, MNIST, GTSRB, RESISC45, Cars], [DTD, EuroSAT, Cars, MNIST, RESISC45], [EuroSAT, GTSRB, MNIST, Cars, RESISC45], [MNIST, Cars, SUN397, DTD, SVHN], [MNIST, SUN397, RESISC45, SVHN, DTD], [SVHN, DTD, Cars, SUN397, MNIST]]
- 6-Tasks: [[GTSRB, RESISC45, DTD, MNIST, SVHN, SUN397], [EuroSAT, GTSRB, Cars, MNIST, DTD, RESISC45], [MNIST, SUN397, SVHN, RESISC45, EuroSAT, DTD], [DTD, MNIST, RESISC45, SVHN, GTSRB, SUN397], [SVHN, RESISC45, EuroSAT, MNIST, GTSRB, DTD], [MNIST, DTD, EuroSAT, Cars, SUN397, GTSRB], [DTD, Cars, SVHN, SUN397, EuroSAT, MNIST], [SVHN, SUN397, RESISC45, GTSRB, EuroSAT, MNIST]]
- 7-Tasks: [[GTSRB, MNIST, Cars, RESISC45, SVHN, DTD, EuroSAT], [Cars, GTSRB, MNIST, SVHN, SUN397, EuroSAT, RESISC45], [Cars, MNIST, SUN397, DTD, EuroSAT, GTSRB, SVHN], [GTSRB, SUN397, EuroSAT, Cars, RESISC45, DTD, MNIST], [SVHN, Cars, GTSRB, MNIST, SUN397, EuroSAT, DTD], [EuroSAT, GTSRB, DTD, RESISC45, SVHN, MNIST, SUN397], [MNIST, SVHN, GTSRB, RESISC45, EuroSAT, DTD, Cars], [EuroSAT, MNIST, GTSRB, DTD, RESISC45, SVHN, SUN397]]